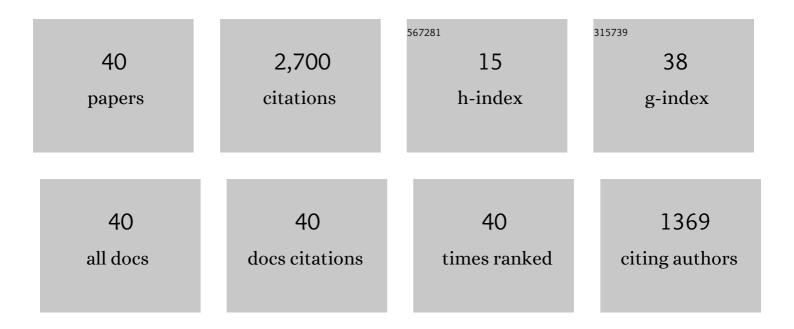


## List of Publications by Year in descending order

Source: https://exaly.com/author-pdf/4355065/publications.pdf Version: 2024-02-01



<u>ϝ~</u>¥<sub>Ϝ</sub>~Ž έΫ@

#	Article	IF	CITATIONS
1	A Fragment of Argoland From East Gondwana in the NE Himalaya. Journal of Geophysical Research: Solid Earth, 2022, 127, .	3.4	3
2	Theoretical Feasibility Analysis of Fast Back-Projection Algorithm for Moon-Based SAR in Time Domain. Applied Sciences (Switzerland), 2022, 12, 3850.	2.5	1
3	U–Pb age, Hf–O isotopes, and geochemistry of the Sardasht ophiolite in the NW Zagros orogen: Implications for the tectonic evolution of Neoâ€Tethys. Geological Journal, 2021, 56, 1315-1329.	1.3	2
4	The youngest matrix of 234ÂMa of the Kanguer accretionary mélange containing blocks of N-MORB basalts: constraints on the northward subduction of the Paleo-Asian Kanguer Ocean in the Eastern Tianshan of the Southern Altaids. International Journal of Earth Sciences, 2021, 110, 791-808.	1.8	34
5	Makran ophiolitic basalts (SE Iran) record Late Cretaceous Neotethys plume-ridge interaction. International Geology Review, 2020, 62, 1677-1697.	2.1	8
6	Accretionary processes and metallogenesis of the Central Asian Orogenic Belt: Advances and perspectives. Science China Earth Sciences, 2020, 63, 329-361.	5.2	97
7	An Image Matching Method for SAR Orthophotos from Adjacent Orbits in Large Area Based on SAR-Moravec. Remote Sensing, 2020, 12, 2892.	4.0	5
8	Age and tectonic setting of the Jingangku Besshi-type volcanogenic massive sulfide deposit from the Northern Shanxi, North China Craton. Precambrian Research, 2020, 350, 105873.	2.7	2
9	Chimney Detection Based on Faster R-CNN and Spatial Analysis Methods in High Resolution Remote Sensing Images. Sensors, 2020, 20, 4353.	3.8	10
10	Iron Isotopes Constrain the Metal Sources of Skarn Deposits: A Case Study from the Han-Xing Fe Deposit, China. Minerals (Basel, Switzerland), 2020, 10, 951.	2.0	2
11	Carboniferous to Early Triassic magmatism and accretion in Alxa (NW China): implications for accretionary orogenesis of the southern Altaids. Journal of the Geological Society, 2020, 177, 997-1012.	2.1	14
12	Late Paleozoic Chingiz and Saur Arc Amalgamation in West Junggar (NW China): Implications for Accretionary Tectonics in the Southern Altaids. Tectonics, 2020, 39, e2019TC005781.	2.8	17
13	Late Paleozoic metallogenesis and evolution of the Chinese Western Tianshan Collage, NW China, Central Asia orogenic belt. Ore Geology Reviews, 2020, 124, 103643.	2.7	12
14	Imaging Karatungk Cu-Ni Mine in Xinjiang, Western China with a Passive Seismic Array. Minerals (Basel,) Tj ETQc	10 0 0 rgB <sup>7</sup> 2.0 rgB <sup>7</sup>	Г /Qverlock 10
15	Deep Structure and Metallogenic Processes of the Altaiâ€Junggarâ€Tianshan Collage in Southern Altaids. Acta Geologica Sinica, 2019, 93, 1163-1168.	1.4	5
16	Geological Characteristics and Metallogenic Setting of Representative Magmatic Cuâ€Ni Deposits in the Tianshanâ€Xingmeng Orogenic Belt, Central Asia. Acta Geologica Sinica, 2019, 93, 1205-1218.	1.4	4
17	Aberration effects in orbital imaging. Remote Sensing Letters, 2019, 10, 816-825.	1.4	3
18	Constructing a High-Accuracy Geometric Model for Moon-Based Earth Observation. Remote Sensing, 2019, 11, 2611.	4.0	15

2

æ~¥æ~Ž éŸ©

#	Article	IF	CITATIONS
19	Late C arboniferous–early P ermian arc magmatism in the southâ€western A lxa T ectonic B elt ( NW C) Tj ETQ Journal, 2019, 54, 1046-1063.	0q1 1 0.784 1.3	4314 rgBT / <mark>O</mark> 18
20	Ages and tectonic implications of the mafic–ultramafic-carbonatite intrusive rocks and associated Cu-Ni, Fe-P and apatite-vermiculite deposits from the Quruqtagh district, NW China. Ore Geology Reviews, 2018, 95, 1106-1122.	2.7	16
21	Final Subduction Processes of the Paleoâ€Asian Ocean in the Alxa Tectonic Belt (NW China): Constraints From Field and Chronological Data of Permian Arcâ€Related Volcanoâ€Sedimentary Rocks. Tectonics, 2018, 37, 1658-1687.	2.8	58
22	Geology, Re-Os and U-Pb geochronology and sulfur isotope of the the Donggebi porphyry Mo deposit, Xinjiang, NW China, Central Asian Orogenic Belt. Journal of Asian Earth Sciences, 2018, 165, 270-284.	2.3	9
23	Anatomy of composition and nature of plate convergence: Insights for alternative thoughts for terminal India-Eurasia collision. Science China Earth Sciences, 2017, 60, 1015-1039.	5.2	62
24	Neoproterozoicâ€Paleozoic Tectonic Evolution of the Northeastern Tarim Block: Constraints from <sup>40</sup> Ar/ <sup>39</sup> Ar Geochronology in the Kuluketage Area, NW China. Acta Geologica Sinica, 2017, 91, 1231-1247.	1.4	1
25	Neoarchean Algoma-type banded iron formation from the Northern Shanxi, the Trans-North China Orogen: SIMS U-Pb age, origin and tectonic setting. Precambrian Research, 2017, 303, 548-572.	2.7	15
26	A Tale of Amalgamation of Three Permo-Triassic Collage Systems in Central Asia: Oroclines, Sutures, and Terminal Accretion. Annual Review of Earth and Planetary Sciences, 2015, 43, 477-507.	11.0	931
27	Late Devonian–early Permian accretionary orogenesis along the North Tianshan in the southern Central Asian Orogenic Belt. International Geology Review, 2015, 57, 1023-1050.	2.1	47
28	Improving the Geolocation Algorithm for Sensors Onboard the ISS: Effect of Drift Angle. Remote Sensing, 2014, 6, 4647-4659.	4.0	11
29	Late Paleozoic metallogenesis and evolution of the East Tianshan Orogenic Belt (NW China, Central) Tj ETQq1 1	0.784314 0.7	• rgBT /Overlo
30	<scp>R</scp> e– <scp>O</scp> s Age of Molybdenite from the <scp>D</scp> aheishan <scp>M</scp> o Deposit in the Eastern <scp>C</scp> entral <scp>A</scp> sian <scp>O</scp> rogenic <scp>B</scp> elt, <scp>NE C</scp> hina. Resource Geology, 2014, 64, 379-386.	0.8	5
31	R e– O s Geochronology on Molybdenites from the D onggebi M o Deposit in the Eastern T ianshan of the C entral A sia O rogenic B elt and its Geological Significance. Resource Geology, 2014, 64, 136-148.	0.8	27
32	<scp><scp>Re</scp></scp> – <scp><scp>Os</scp> Isotopic Age of the <scp>H</scp>ongqiling <scp><scp>Cu</scp></scp>–<scp><scp>Ni</scp> Sulfide Deposit in <scp>J</scp>ilin Province, <scp>NE C</scp>hina and its Geological Significance. Resource Geology, 2014, 64, 247-261.</scp></scp>	0.8	14
33	Neoarchean Algoma-type banded iron formations from Eastern Hebei, North China Craton: SHRIMP U-Pb age, origin and tectonic setting. Precambrian Research, 2014, 251, 212-231.	2.7	44
34	Tectonic implications of Re-Os dating of molybdenum deposits in the Tianshan–Xingmeng Orogenic Belt, Central Asia. International Geology Review, 2014, 56, 985-1006.	2.1	8
35	Paleozoic multiple accretionary and collisional tectonics of the Chinese Tianshan orogenic collage. Gondwana Research, 2013, 23, 1316-1341.	6.0	874
36	Palaeozoic porphyry Cu–Au and ultramafic Cu–Ni deposits in the eastern Tianshan orogenic belt: temporal constraints from U–Pb geochronology. International Geology Review, 2013, 55, 842-862.	2.1	11

æ~¥æ~Ž éŸ©

#	Article	IF	CITATIONS
37	The Liuyuan complex in the Beishan, NW China: a Carboniferous–Permian ophiolitic fore-arc sliver in the southern Altaids. Geological Magazine, 2012, 149, 483-506.	1.5	122
38	In-situ U–Pb, Hf and Re–Os isotopic analyses of the Xiangshan Ni–Cu–Co deposit in Eastern Tianshan (Xinjiang), Central Asia Orogenic Belt: Constraints on the timing and genesis of the mineralization. Lithos, 2010, 120, 547-562.	1.4	156
39	REE mineralization related to carbonatites and alkaline magmatism in the northern Tarim basin, NW China: implications for a possible Permian large igneous province. International Journal of Earth Sciences, 0, , 1.	1.8	Ο
40	Rheniumâ€Osmium Isotope Constraints on the Origin of the Tianyu Cuâ€Ni Deposit in the East Tianshan Orogenic Belt, Xinjiang, NW China. Acta Geologica Sinica, 0, , .	1.4	0